Computers & Fluids 39 (2010) 359–371

Contents lists available at ScienceDirect

Computers & Fluids

journal homepage: www.elsevier.com/locate/compfluid

Effects of wall temperature on boundary layer stability over a blunt cone at Mach 7.99

Xian Liang [a,*], Xinliang Li [b,*], Dexun Fu [b], Yanwen Ma [b]

[a] Shanghai Institute of Applied Mathematics and Mechanics, Shanghai University, Shanghai 200072, China
[b] LNM, Institute of Mechanics, Chinese Academy of Sciences, Beijing 100190, China

ARTICLE INFO

Article history:
Received 4 December 2008
Received in revised form 29 July 2009
Accepted 24 September 2009
Available online 2 October 2009

Keywords:
Hypersonic
Linear stability theory
Mack mode
Shock-fitting methods
Receptivity

ABSTRACT

Effects of wall temperature on stabilities of hypersonic boundary layer over a 7° half-cone-angle blunt cone are studied by using both direct numerical simulation (DNS) and linear stability theory (LST) analysis. Four isothermal wall cases with $T_w/T_0 = 0.5, 0.7, 0.8$ and 0.9, as well as an adiabatic wall case are considered. Results of both DNS and LST indicate that wall temperature has significant effects on the growth of disturbance waves. Cooling the surface accelerates unstable Mack II mode waves and decelerates the first mode (Tollmien–Schlichting mode) waves. LST results show that growth rate of the most unstable Mack II mode waves for the cases of cold wall $T_w/T_0 = 0.5$ and 0.7 are about 45% and 25% larger than that for the adiabatic wall, respectively. Numerical results show that surface cooling modifies the profiles of $\rho\frac{du_L}{dy_n}$ and temperature in the boundary layers, and thus changes the stability characteristic of the boundary layers, and then effects on the growth of unstable waves. The results of DNS indicate that the disturbances with the frequency range from about 119.4 to 179.1 kHz, including the most unstable Mack modes, produce strong mode competition in the downstream region from about 11 to 100 nose radii. And adiabatic wall enhances the amplitudes of disturbance according to the results of DNS, although the LST indicates that the growth rate of the disturbance of cold wall is larger. That because the growth of the disturbance does not only depend on the development of the second unstable mode.

1. Introduction

Prediction of laminar–turbulent transition of hypersonic boundary layer is very important in aerodynamic designs of hypersonic vehicles. However, although decades researches, there is still no reliable mathematical model to accurately predict locations of transition. And the mechanism of hypersonic boundary layer transition is still unclear. The most widely used transition prediction method is e^N method, which suggests that the transition occurs when the amplitude of most unstable disturbance increased to e^N times. The quantity N is obtained by integrating the linear growth rate from the first neutral-stability point at a location somewhere downstream on the body, but e^N represents nothing more than an amplitude ration. Here N usually is a number from experiment, which belongs to [9,11] for incompressible boundary layer. However, the limit of e^N method is that it does not consider the initial generation of disturbance, in fact the transition process depends on the initial disturbance which is the area of receptivity study. As addressed in Reed and Saric [1], the role of receptivity, not accounted for in linear stability theory, is key to the overall process as it defines the initial disturbance amplitude at the first neutral-stability point. In order to improve transition prediction method, it is important to study the mechanism of receptivity. Saric [2–4] and Mack [5,6] reviewed the historical progress in the research of receptivity, boundary layer stability and discussed the importance of these works in the study of transition.

Generally the process of boundary layer transitions in external flow can be divided into fours stages, which are receptivity linearly growth, nonlinearly growth, transition and full development. And the first two stages play important roles in transition prediction, because the last two stages are much shorter than the first two ones. In the case of enough strong forcing environment disturbance, the above process turns into bypass type transition [7], and the first one stage, even first two stages, will be bypassed. Receptivity research, which study how the forcing environmental disturbances enter into boundary layer and produce unstable wave that further to develop and induce typical unstable wave in boundary layer, is of importance to understand and predict transition [7–10]. The process of hypersonic boundary layer receptivity to free-stream disturbance is much more complex than incompressible or subsonic boundary layer receptivity [5,11,12]. The later one has been relatively well understood, while the former is not so clear and still an active research [2,4]. At present, investigation on stability and transition of hypersonic boundary layer is mainly based on the linear stability theory (LST) [6] which mainly

* Corresponding authors. Tel.: +86 10 82543925; fax: +86 10 82543913.
E-mail addresses: liangx_yan@126.com (X. Liang), lixl@lnm.imech.ac.cn (X. Li).

0045-7930/$ - see front matter © 2009 Elsevier Ltd. All rights reserved.
doi:10.1016/j.compfluid.2009.09.015

considers the growth and decay of normal modes in hypersonic boundary layer. According to LST, the transition is a result of exponential growth of the most unstable normal modes, which is foundations of e^N method [5,13–15]. Mack [6] found that the hypersonic boundary layer stability different from that in low speed flows, and transition prediction for hypersonic boundary layers is much more difficult than that for low speed ones. There is only one unstable mode (T–S waves) in low speed boundary layer. With the increasing of the free-stream Mach number, high frequency modes appears, and the Mack II mode becomes the most unstable disturbance wave when free-stream Mach number is high enough [5,16]. Tumin [17] has proposed a numerical method to solve a Cauchy problem based on the linear disturbance equations with local parallel flow approximation. He has decomposed perturbations into modes of continuous and discrete spectra, which helps to elucidate underlying mechanisms that are important in laminar–turbulent transition scenarios.

Recently, Zhong et al. [18–23] have completed a series of numerical studies of receptivity of supersonic and hypersonic boundary layer over flat plate and blunt cone by using both LST and numerical simulation with high-order shock-fitting method [18]. Zhong et al. investigated the linear instability characteristics of the boundary layer wave modes and their mutual resonant interaction. They thought that the stable wave modes, which are not Mack modes, play critical roles in transferring wave energy between the acoustic wave and the unstable second Mack mode. They proposed a resonant mechanism numerically that finally leads to unstable Mack mode in boundary layer, and further applied this opinion to study the boundary layer receptivity of Mach 7.99 to free-stream acoustic waves flow over a blunt cone [23]. In Zhong et al.'s studies, only adiabatic wall is considered. However, in many cases the wall is proximately isothermal or between adiabatic and isothermal. Effects of wall temperature to instability of disturbance waves is also of great importance in transition prediction and controls of hypersonic boundary layer transition.

Wall temperature produces a notable effect on disturbance waves. Mack [5] has pointed out that the effect of cooling wall could be regarded as disturbance source in flat plate. Also for hypersonic Mach number, the unstable second mode can promote instability amplification over the whole temperature range. Stetson [24–27] has performed a series experiments on hypersonic over a cone. For effect of wall temperature, he draw a conclusion that cooling the surface stabilized the first mode disturbance and destabilized the second mode disturbance, as predicted by LST. The second mode disturbance growth rates on the water-cooled cone ($T_w/T_0 = 0.42$, T_w: wall temperature, T_0: total temperature) were approximately 50% larger than those on the uncooled cone ($T_w/T_0 = 0.82$). The transition Reynolds number changed from approximately 4.4×10^6 (uncooled) to approximately 3.2×10^6 (cooled). Stability of hypersonic boundary layer on a cone is much different from that on a plane according to relevant hypersonic wind tunnel experiments [26], so it is necessary to complete more investigation on this area. However, it is still lack of systematic numerical simulation of boundary layer stability over blunt cones with wall temperature effects.

This paper presents a numerical study on the stability of boundary layer for hypersonic flow, mainly considering the effect of wall temperature. The aim of this paper is to investigate some new physics phenomena in high Mach number flows that can lead to transition. The flow conditions were duplicated from the experiments of Stetson and Kimmel [25]. Two critical problems are discussed in this paper. The first one is attempt to interpret how the wall temperature influences mean flow profile in hypersonic boundary layer. And the second one is how the wall temperature influences the evolution of disturbance waves.

2. Governing equations and numerical methods

Before introducing the governing equations and flow conditions, we prefer to describe the conception of subscript and superscript used in present paper. Subscripts '*w*' denote the wall condition, '*o*', total conference condition, '∞', free-stream and '*e*', outer edge of boundary layer. Superscript '$*$' denotes the dimensional flow variable. In this paper, the dimensionless flow variables are denoted by the same dimensional notation, but without the superscript '$*$'.

The three-dimensional Navier–Stokes equations for steady and unsteady hypersonic flow computation are transformed into the general curvilinear coordinates (ξ, η, ζ) from the Cartesian coordinates (x, y, z) as

$$\frac{\partial (J^{-1}U)}{\partial t} + \frac{\partial E'}{\partial \xi} + \frac{\partial F'}{\partial \eta} + \frac{\partial G'}{\partial \zeta} + \frac{\partial E'_v}{\partial \xi} + \frac{\partial F'_v}{\partial \eta} + \frac{\partial G'_v}{\partial \zeta} = 0, \tag{1}$$

where

$$E' = \frac{E\xi_x + F\xi_y + G\xi_z + U\xi_t}{J}, \quad F' = \frac{E\eta_x + F\eta_y + G\eta_z + U\eta_t}{J},$$
$$G' = \frac{E\zeta_x + F\zeta_y + G\zeta_z + U\zeta_t}{J}, \quad E'_v = \frac{E_v\xi_x + F_v\xi_y + G_v\xi_z}{J},$$
$$F'_v = \frac{E_v\eta_x + F_v\eta_y + G_v\eta_z}{J}, \quad G'_v = \frac{E_v\zeta_x + F_v\zeta_y + G_v\zeta_z}{J}.$$

We non-dimensionalize the flow velocities by the free-stream velocity U^*_∞, length scales by the nose radius r^*_n, density by ρ^*_∞, pressure by $\rho^*_\infty U^{*2}_\infty$, temperature by T^*_∞, time by r^*_n/U^*_∞.

In present investigation, the amplification of disturbance waves in the free-stream is as small as order of 10^{-4}. In order to resolve such small disturbance and improve compute precision, a high-order-accurate shock-fitting finite difference method is applied which is based on the fifth-order upwind compact schemes, the sixth-order central schemes and the third-order Runge–Kutta schemes. The grid surface $\eta = 1$ is body surface, and $\eta = \eta_{max}$ is the bow shock as the outer boundary. For the blunt cone, the grid surface of η is unsteady and the grid-lines turn to be shorter or longer with time, but the grid surfaces of ξ and ζ are fixed during computation. The unsteady flow is simulated by using the moving grid method, in which η_t and $\partial(J^{-1})/\partial t$ are not zero. The present shock-fitting method is much different from that of Zhong's [18] in resolving of the characteristic compatibility relation formula. The details of the numerical methods can be found in paper [28].

3. Flow conditions

The flow conditions in present paper are the same as those of Stetson and Kimmel [25] experiment, where the data of laminar boundary layer stability on a cone with half-angle 7° at Mach 7.99 are proposed. The specific flow conditions [23] are:

$M_\infty = 7.99$, $T^*_0 = 750$ K, $p^*_0 = 4 \times 10^6$, $p^*_\infty = 413$ Pa,
$Re_\infty/ft = 2.5 \times 10^6$, $Re_{rn} = \rho^*_\infty U^*_\infty r^*_n/\mu^*_\infty = 31,250$,
$\gamma = 1.4$, $Pr = 0.72$, gas constant $= 286.94$ Nm kg^{-1} K^{-1},
Blunt cone half-angle: $\theta = 7°$, zero flow angle of attack,
Spherical nose radius: $r^*_n = 3.81 \times 10^{-3}$ m,
Parameters in Sutherland's viscosity law: $T^*_0 = 288$ K, $C = 110.33$ K, $\mu^*_0 = 0.17894 \times 10^{-4}$ kg ms^{-1},

where T^*_0 and p^*_0 are free-stream total pressure and free-stream total temperature, respectively. The total length of the cone of the present experimental mode is $l^* = 1.143$ m. The corresponding Reynolds number at this length is $Re_l = 9.375 \times 10^6$.

Further more, before introducing the boundary conditions, we prefer to interpret recovery temperature, T_r, on the cone for adiabatic wall in our computation. T_r was computed by

$$T_r = T_e\left(1+\frac{\gamma-1}{2}M_e^2\sqrt{Pr}\right). \quad (2)$$

T_e and M_e, the temperature and Mach number on outer edge of boundary layer, are equal to about 1.34 and 6.8, respectively, and T_r equal to about 646 K for adiabatic wall with above flow conditions. So the wall temperature T_w over total temperature T_0 equal to 0.5, 0.7, 0.8, 0.9 are identical with the wall temperature T_w over recovery temperature T_r equal to 0.58, 0.81, 0.93, 1.05, respectively. So the first three wall temperature conditions denote the cooling wall and the last one denoted the heating wall, however heated slightly. And the former expression is employed in present paper. No-slip boundary conditions are used on the body surface.

In this paper, the origin of the Cartesian system (x, y, z) is located at stagnation point of the nose spherical cone, where the x-coordinate points from left to the right along the centreline of the axis-symmetric cone. Meanwhile, a natural coordinate s corresponding to x is used to measure the dimensionless curve length of a surface location started from the stagnation point. The non-dimensional s and x, which are normalized by the nose radius r_n^*, are related to each other by the following relation:

$$x = \begin{cases} 1-cos(s) & s \leqslant \frac{\pi}{2}-\theta \\ (s-\frac{\pi}{2}+\theta)cos(\theta)-sin(\theta)+1 & s > \frac{\pi}{2}-\theta \end{cases}, \quad (3)$$

where θ is the radian of the half-angle of the cone.

4. Numerical results and discussion

4.1. Numerical methods test

Before our computation, some computational results were carried out to compare with results of Ma and Zhong [23] to verify the validity of the present numerical method. Moreover, the results of Ma and Zhong agree well with those of experiments [25] and Herbert and Esfahanian [31]. The computational surface is 2D axis symmetrical blunt cone with adiabatic wall and $Re_m = 33,449$, while the other computational parameters are set as same as those in last section. Fig. 1 shows the position of bow shock and the comparison of numerical vorticity jump with theoretical value along the bow shock. It clearly indicates that the numerical results agree well with theoretical values of vorticity jump. It also shows that the current numerically computed bow shock agrees very well with the solution of Ma and Zhong. Fig. 2(a) shows the wall pressure along the cone surface, which indicates that the present numerical results agree well with Zhong's. The figure shows that the wall pressure decreases sharply from the maximum value at stagnation point when s increasing from 0 to about 15, and then increases when s increasing from about 15 to 80 as follow expands around nose region. The wall pressure is almost a constant for about $s > 80$. Due to the surface curvature discontinuity, flows show overexpansion in the junction region between the spherical nose and the straight cone, and go through a recompression region along the downstream cone surface. As a result, there is slight adverse pressure gradient along the surface location after the junction. Meanwhile there exist similar change of wall temperature which only has slightly adverse temperature gradient and sharply decreases at nose region. This can be found in Fig. 2(b). Generally, the present method can give a quite well surface value. Fig. 3 shows the comparison of the tangential velocities profiles across the boundary layer at a surface location of $s = 94$ and 128. These comparison indicate that the current numerical results agree very well with those obtained by Zhong's calculation, so the present computa-

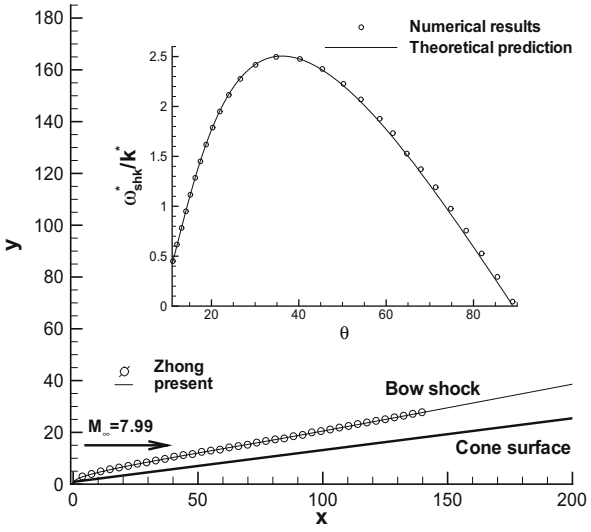

Fig. 1. Shock position and comparison of vorticity jump.

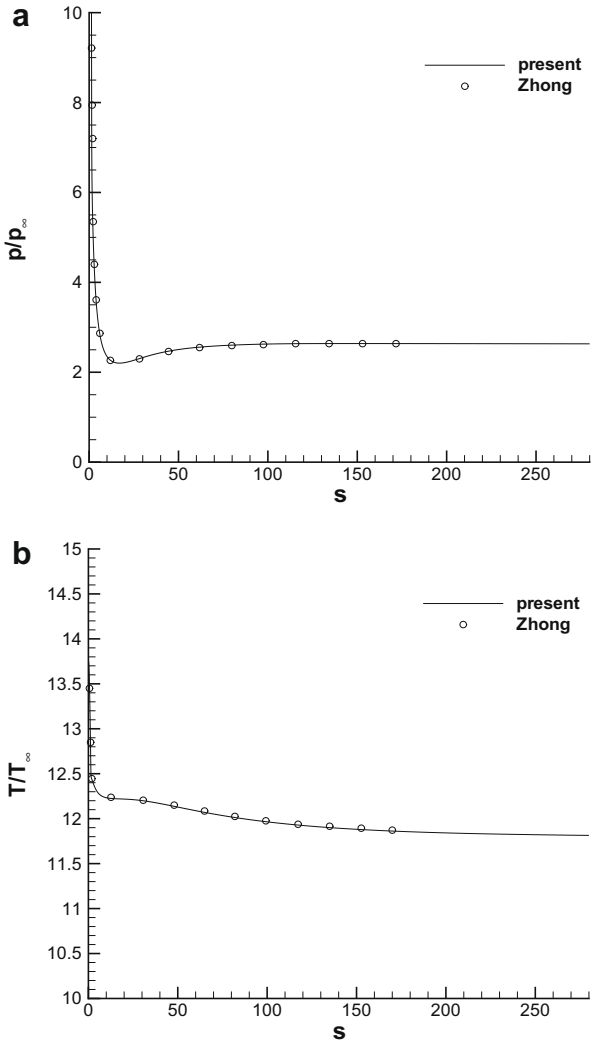

Fig. 2. (a) Steady pressure and (b) temperature distributions along the cone surface.

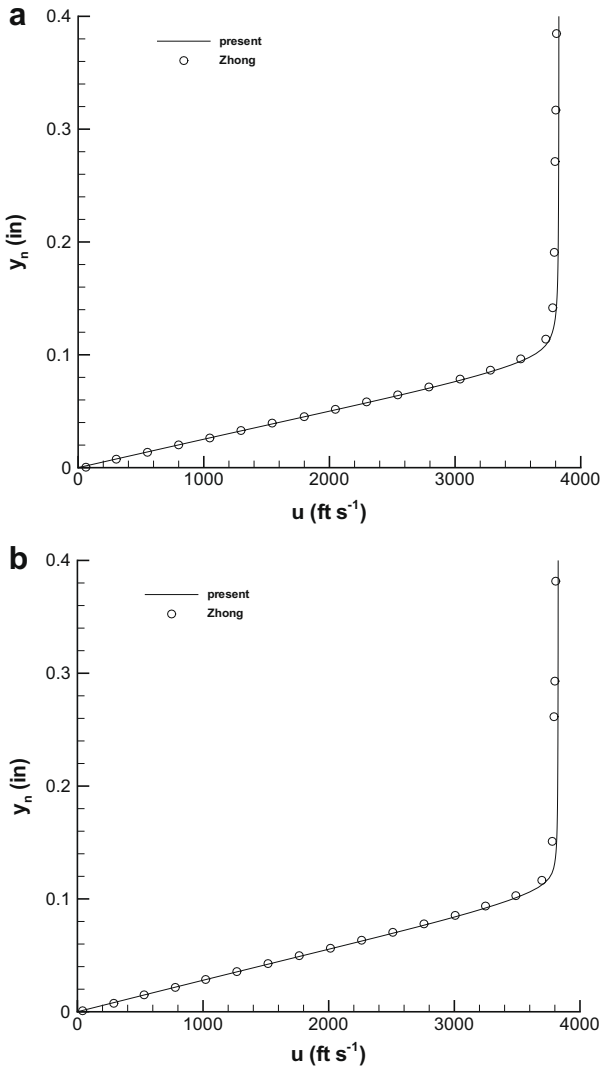

Fig. 3. Tangential velocity profiles along the wall-normal direction at the surface locations of 94 and 128 nose radii.

tion also can obtain well results through the boundary layer, thus satisfied the accuracy requirement of computation.

4.2. Steady flow for different wall temperature conditions

From this part, the computing parameters showed in Section 3 are adopted. Fig. 4 shows the comparison of the tangential velocity, obtained under adiabatic wall and cooling wall ($T_w/T_0 = 0.7$) conditions, respectively, at different surface location. This figure shows that boundary layers for adiabatic wall are thicker than that of the cold wall ($T_w/T_0 = 0.7$) at the same locations. According to Mack [6], the wavelength of the most unstable wave is approximately twice the boundary layer thickness, and the change of boundary layer thickness due to difference wall temperature leads to the change of instability characteristic. After interacting with shock-wave, the disturbance entering into boundary layer induces the disturbances, which further to interact with boundary layer and finally to generate the most unstable mode dominating the transition position. Su and Zhou [29] has calculated transition location of Mach 6 flow over a blunt-cone with 5° half cone angle by using e^N method. Their results indicated that the wall temperature has significant effects on the transition, and transition location of the

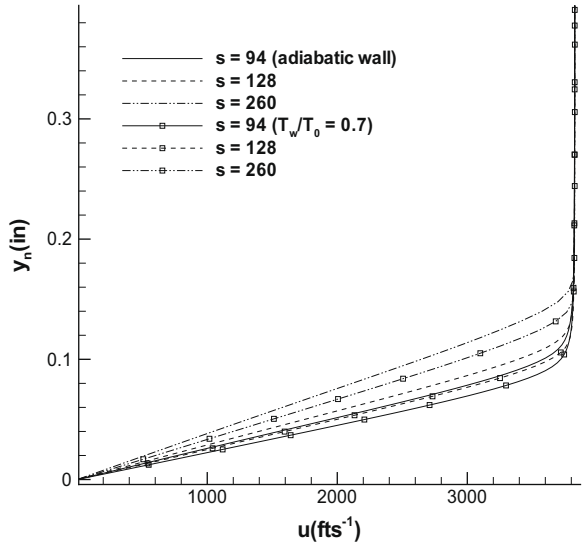

Fig. 4. Effects of wall temperatures on tangential velocity profiles along the wall-normal direction.

boundary layer with adiabatic wall is 60% larger than that of the cooling wall.

$\rho \frac{du_t}{dy_n}$ is one of the several parameters to characterize the entropy layer which come into being after the bow shock and near the nose region. Fig. 5 shows the contours of the $\rho \frac{du_t}{dy_n}$ computed with adiabatic wall condition. A obvious peak exists in the contour lines outside the boundary layer. Fig. 6 shows the profiles of $\rho \frac{du_t}{dy_n}$. Furthermore the positions where $d(\rho \frac{du_t}{dy_n})/dy = 0$ are called generalized inflection points(GIPs). Lees and Lin [30] showed that existence of a GIP is a necessary condition for the inviscid instability in a compressible boundary layer.

Fig. 6 demonstrates the values of the $\rho \frac{du_t}{dy_n}$ and positions of the GIPs effected by wall temperatures. The difference of profiles outside the boundary layer are slight for different wall temperature, however distinctive inside the boundary layer. In Fig. 6(a)–(c), the peaks outside the boundary layer are clearly showed on the profile of $\rho \frac{du_t}{dy_n}$ from the nose region to downstream location at about $s = 32.87$ where the peak outside the boundary layer has

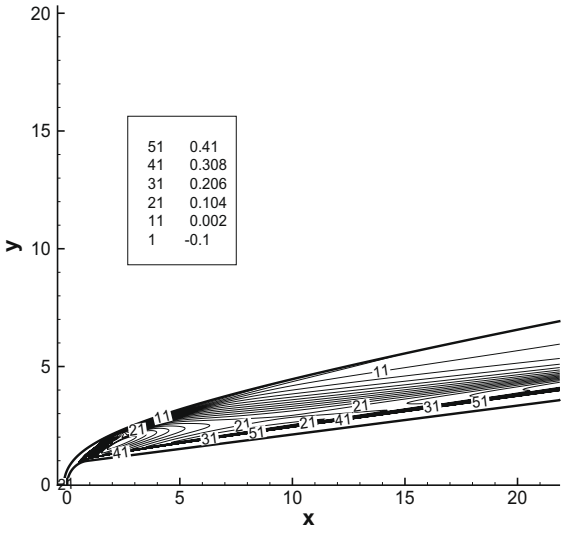

Fig. 5. Contours of $\rho \frac{du_t}{dy_n}$ for adiabatic wall.

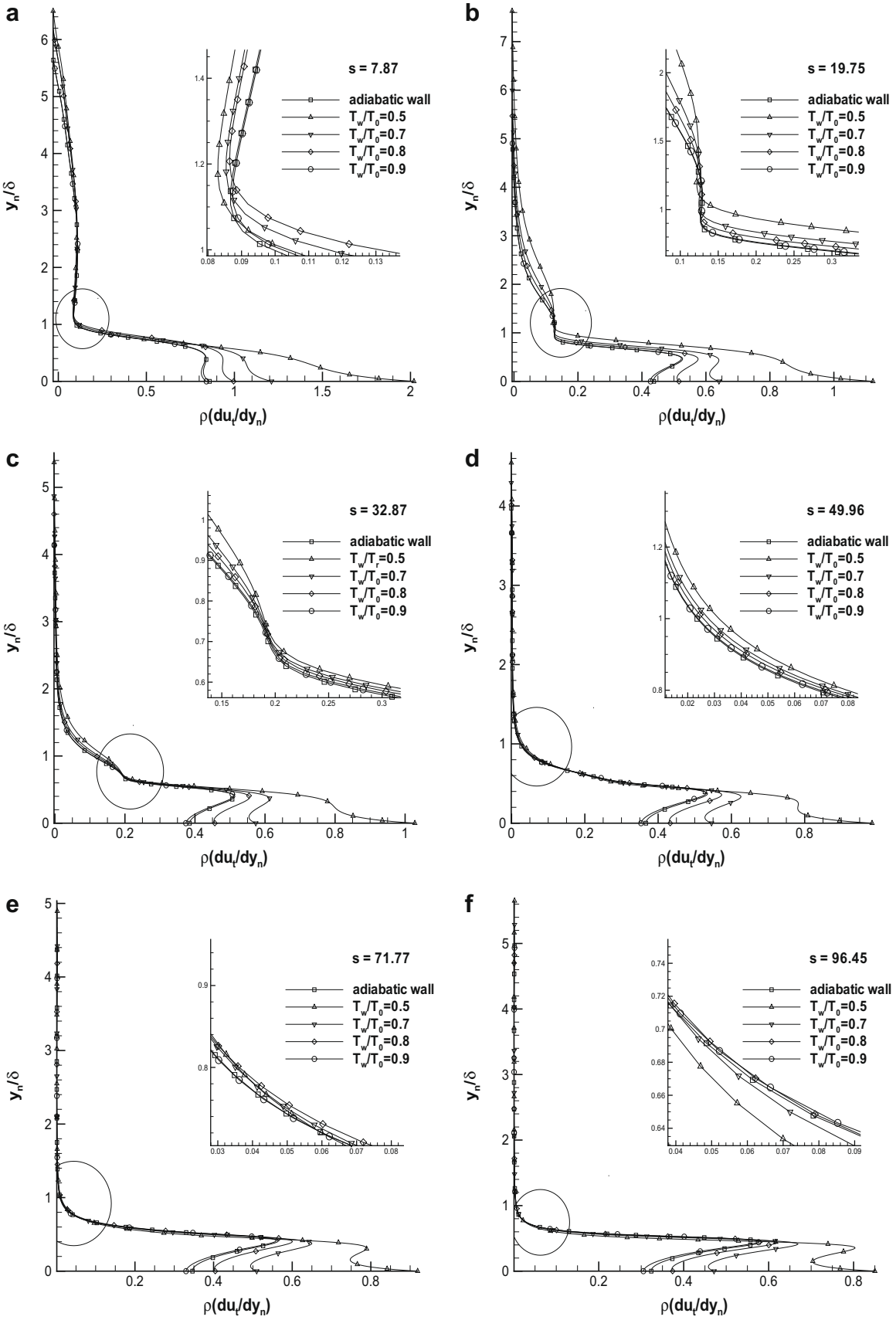

Fig. 6. The profiles of $\rho\frac{du_t}{dy_n}$ along the wall-normal at different surface locations (y-axis is normalized by boundary layer thickness δ).

been swallowed by the boundary layer. Fig. 6(a) shows the profiles in favorable pressure gradient region, while (b)–(d) in adverse pressure gradient region. Fig. 6(a) indicates that firstly, the value of $\rho\frac{du_t}{dy_n}$ on the wall are affected seriously by wall temperature, which is about 110% higher at $T_w/T_0 = 0.5$ and 50% higher at $T_w/T_0 = 0.7$ than that for adiabatic wall. Secondly, two GIPs exist in boundary layer in favorable pressure gradient region for adiabatic wall conditions. Indeed, for heating wall ($T_w/T_0 = 0.9$), it is similar to the results for adiabatic wall. Further down streamwise, after the flow enter into adverse region at about $s > 19$, the profiles of $\rho\frac{du_t}{dy_n}$ appear some new changes. Fig. 6(b)–(d) shows that existence of adverse pressure gradient contribute to the progress of forming two GIPs in boundary layer for cold wall ($T_w/T_0 = 0.7$), meanwhile, only one GIP exists in boundary layer for adiabatic wall and heating wall. In other word, one GIP disappears from favorable to adverse pressure gradient region for adiabatic and heating wall. Additionally, there is no GIP for cold wall at $T_w/T_0 = 0.5$ for about $s < 32.67$ in boundary layer. It indicates that the flow is stable in this region according to theory of Lees and Lin [30]. When about $s > 71.77$, Fig. 6(e) and (f) shows that only one GIP exists in boundary layer for wall temperature cases of $T_w/T_0 = 0.8$, 0.9 and adiabatic wall condition, but there still exist two GIPs for cold walls at $T_w/T_0 = 0.5$, 0.7. The similar phenomena in the flat plate boundary layer on Mach 3 has been reported by Mack [5]. Generally speaking, cooling the surface leads to two GIPs which produce some instable factors to the development of disturbance in boundary layer and increases uncertainty and complex to stability analysis.

4.3. Linear stability theory(LST)

LST based on the assumption of local parallel flow has obtained satisfied results in incompressible flow and subsonic flat plate flow. That can be used to identify the main components of stability characteristics of boundary layer disturbances. Because of neglecting increase of boundary layer along streamwise, such increase is markedly in some special flow, for instance, the flat plate with angle, flow around a cone, therefore LST can not provide additional information produced by nonparallel effect. In this section, we introduce a length scale of the boundary layer thickness $L^* = \sqrt{\mu^*_\infty s^*/\rho^*_\infty u^*_\infty}$, where $s^* = r^*_n s$. A local Reynolds number, based on the L^*, is defined as $R = \rho^*_\infty u^*_\infty L^*/\mu^*_\infty$. Dimensionless angular frequency ω and wave number α which are normalized by u^*_∞ and L^*

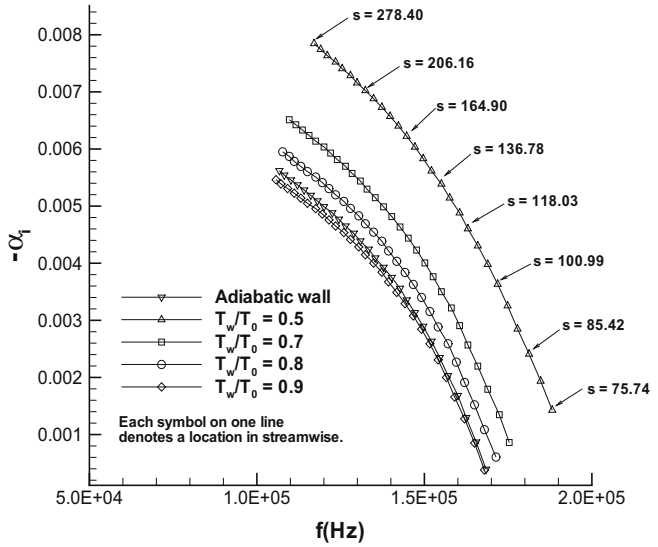

Fig. 8. Comparison of maximum growth rate of Mack II mode along the streamline for different wall temperatures.

are defined as $\alpha = \alpha^* L^*$ and $\omega = \omega^* L^*/u^*_\infty$, respectively. And the relation between the dimensionless frequency F and ω is $\omega = 10^{-6}FR$. The linear fluctuations of flow variables are decomposed into the following normal mode form:

$$f' = \hat{f}(y_n)exp[i(\alpha s - \omega t)], \tag{4}$$

where the variable f stands for any of the independent flow variable u, v, w, p, ρ, T. $\alpha = \alpha_r + i\alpha_i$ is a streamwise complex wavenumber, $\hat{f}(y_n)$ is the complex shape-function of the disturbance, n and s are the local natural coordinates along the wall-normal and surface directions, respectively. In a spatial linear stability analysis, for a given frequency ω, α and $\hat{f}(y_n)$ are computed as eigenvalue and eigenfunction of the stability equation. The real and imaginary parts of α, α_r and α_i represent the spatial wave number and growth rate of a wave mode, respectively. A linear wave mode is unstable when α_i is negative.

Fig. 7 compares the present growth rates computed with different wall temperatures with the results of Herbert's [31], Malik's

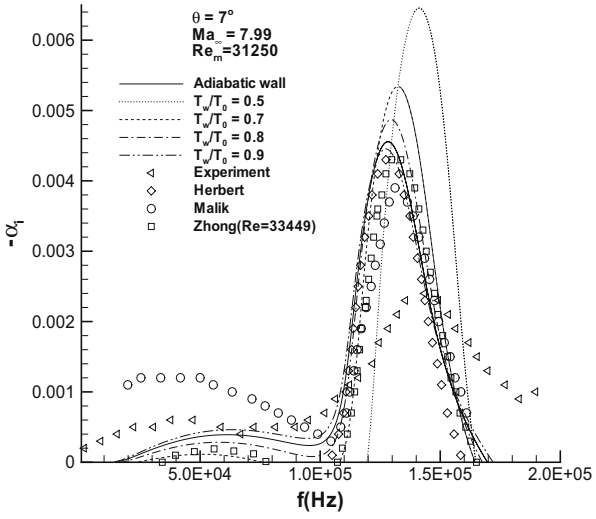

Fig. 7. Comparison of the growth rates of the disturbance predicted by LST at surface location $s = 175$.

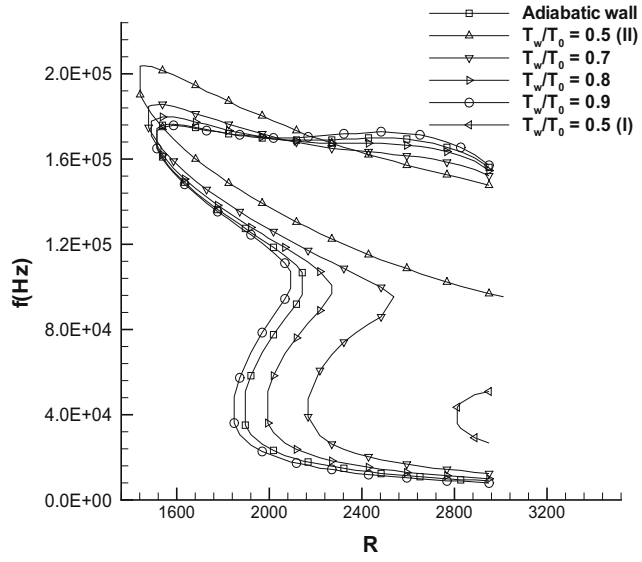

Fig. 9. Comparison of neutral curve for different wall temperatures.

[13] and Zhong's obtained under adiabatic wall condition, while the other parameters are the same as ours. The present results of the growth rate of Mack II mode computed with adiabatic wall agrees well with that of Herbert's, Malik's and Zhong 's et al. (Reynolds number in Zhong's paper is $Re_{rn} = 33,449$ which is about 7% larger than present value of 31,250. In fact, such difference can not lead notable difference in hypersonic flow at $Ma = 7.99$). In general, the amplification rates computed with adiabatic wall well agree with other's. As showed in Fig. 7, the maximum value of the growth rates of Mack II mode are -0.0064, -0.0054, -0.0049, -0.004 and -0.0046 corresponding to $T_w/T_0 = 0.5$, 0.7, 0.8, 0.9 and adiabatic wall at surface location about $s = 175$, respectively. The comparison indicates that cooling the surface promotes the instability and accelerates the growth of the unstable Mack II mode. Meanwhile, the maximum value of the growth rates of the first mode are -0.0001, -0.0003, -0.0005 and -0.0004 corresponding to $T_w/T_0 = 0.7$, 0.8, 0.9 and adiabatic wall, respectively. It indicates that cooling the surface decreases the growth of the first mode, but adiabatic and heating wall promote it. Moreover, the cold wall at $T_w/T_0 = 0.5$ restrains the growth of the first unstable mode completely at above mentioned location. So it can be concluded that cooling the surface accelerates the growth of unstable Mack II mode and restrains the first mode and the value of growth rate of Mack II mode is much greater than that of the first mode. So Mack II mode is a dominant unstable mode in hypersonic boundary layer over a cone according to LST.

Fig. 8 compares the maximum growth rate curves of Mack II mode along the streamwise for different wall temperature. This indicates the relationship between the wall temperature and the evolution of most unstable mode in boundary layer. Lines denote the different results computed with different wall temperature and each symbol on each line denotes a surface location. The results indicate that, firstly, the growth rate of most unstable Mack II mode continuously increase with increasing s. Secondly, the growth rate of most unstable Mack II for cold wall is larger than that of adiabatic wall at any same location through all streamwise. Thirdly, the larger growth rate for the second unstable mode can be produced by decreasing wall temperature. Additional, the wavelength of the Mack II mode increases (or frequency decrease) with increasing s and the wavelength of the first mode is relative unchanged with increasing s according to present computation.

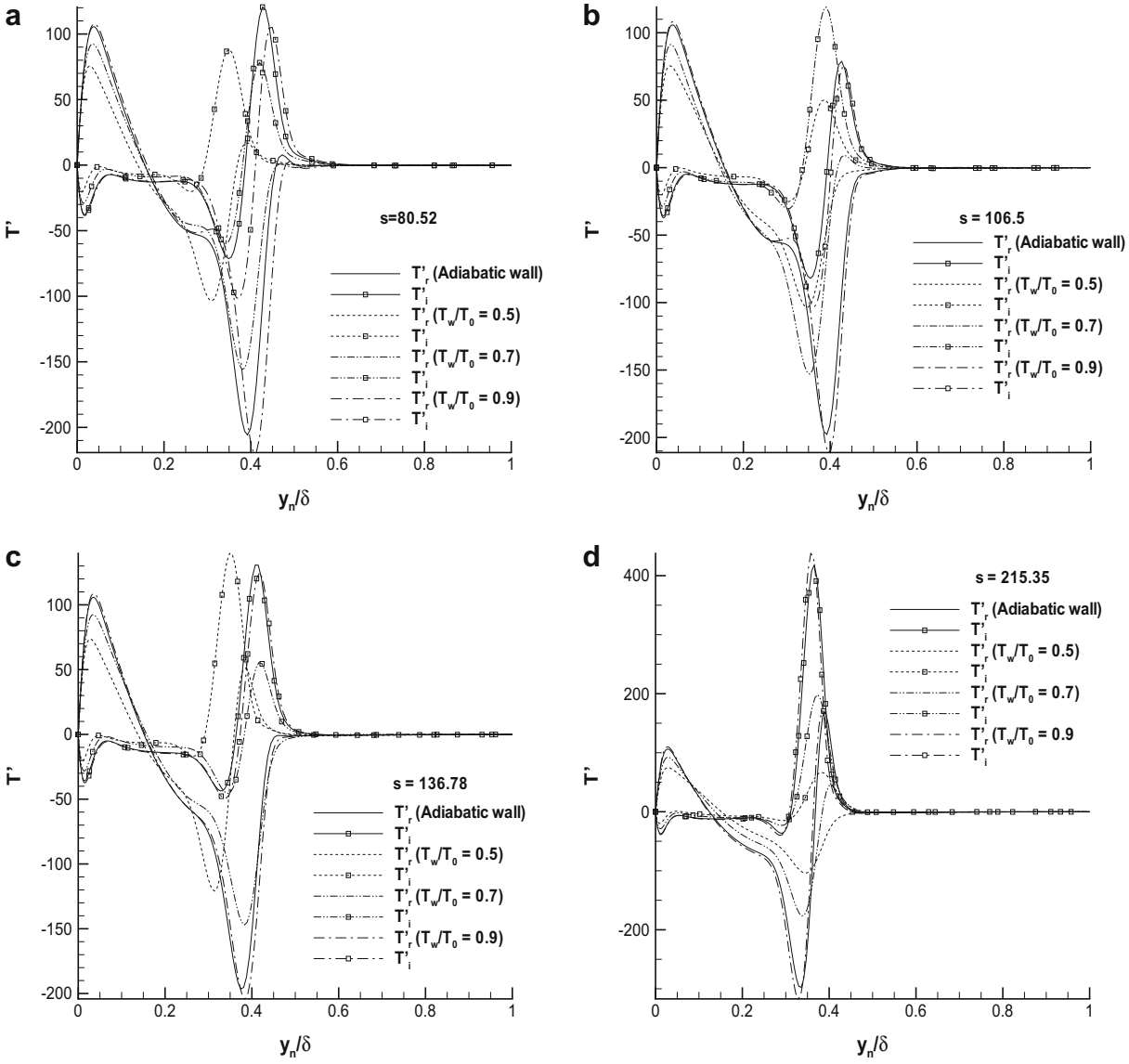

Fig. 10. Distribution of temperature eigenfunction along the wall-normal at four surface location for different wall temperatures (x-axis is normalized by boundary layer thickness δ).

Neutral curve which acts critical roles in stability analysis provides the growth interval of unstable mode in 2D cases It is the first step to predict transition by using e^N method. Fig. 9 compares the neutral curves obtained by adopting different wall temperature. It indicates that the neutral curve depended on the wall temperature closely. Fig. 9 indicates that the starting location where the disturbance wave access to the neutral curve for cooling wall is larger than that for adiabatic wall. The starting locations for the first mode are about $s = 250$, 149, 128, 108 and 118 corresponding to $T_w/T_0 = 0.5, 0.7, 0.8, 0.9$ and adiabatic wall, respectively. This difference leads to the disturbance growth for adiabatic wall, which is earlier than that for cooling wall. Meanwhile, the difference of such starting positions for the Mack II mode is not so obviously, about s from 64 to 72. But the unstable interval starting from this point is very short and mainly affects on high frequency wave (at about $f^* > 1.7 \times 10^5$) which can not obtain enough growth. Another notable difference is that the neutral curve expands to high frequency at $T_w/T_0 = 0.5$, and 0.7. What effect will be produced by such expansion is not clear at present.

The eigenfunction (shape-function) reflects the shape of disturbance wave and its distribution along normal direction to the wall surface. Fig. 10 compares temperature eigenfunction for different wall temperatures at four surface locations. The figures show that the temperature eigenfunction of cold wall has much difference from that for adiabatic wall. Fig. 10(a)–(c) indicates that the fluctuation of the eigenfunction is closer to the wall surface at $T_w/T_0 = 0.5$ than that for adiabatic wall for about $s < 136.78$. And the real part and imaginary part of eigenfunction for cold wall are much difference from that for adiabatic wall for $s = 215.35$. So the wall temperature affect the distribution of the disturbance wave, which leads to different stability characteristic.

The present LST analysis indicates that stability of a blunt cone at $Ma = 7.99$ with zero attack angle and 7° half cone angle is sensitive to the wall temperature. Cooling surface accelerates the growth of the second unstable mode and decreases or even restrains the first mode. Especially the significant difference of temperature eigenfunction indicates that the changes of the thermal conductive characteristic can affect on the evolution of disturbance significantly in boundary layer in hypersonic flow.

4.4. Growth of unstable mode in boundary layer

In order to investigate the spatial evolution of disturbance waves along streamwise in boundary layer, a set of free-stream forcing waves with a mixture of 15 independent planner fast acoustic waves of different frequency are introduced at shock wave boundary. These fast acoustic wave frequencies are

$$f_n^* = nf_1^*, \quad (n = 1, 2, \ldots, 15), \tag{5}$$

where the lowest frequency $f_1^* = 14.92(\text{kHz})$ $(F_1 = 9.04)$ and the remaining 14 frequencies are multiples f_1^* given by (5). So the highest frequency of the fast acoustic wave is $f_{15}^* = 223.8$ kHz $(F_{15} = 135.5)$. These fast acoustic waves, including relative amplitude, frequencies and phase angle of each disturbance wave chosen according to Stetson's experiment [25] are listed in Table 1. This data also can be found in [23]. The total amplitude of forcing disturbance is $\varepsilon = 6.2578 \times 10^{-4}$, a sufficiently small value to guarantee the receptive process falls in the linear regime. And the amplitudes of forcing wave for low frequencies are about one order higher than that of high frequencies.

4.4.1. Development of disturbance in boundary layer

Fig. 11 shows the distribution of the wall pressure disturbance in streamwise. For different wall temperature conditions, the changes of pressure disturbance are similar to a certain extent.

Table 1
Forcing acoustic wave components of 15 frequencies in the free-stream.

n	A_n	F_n	f^* (kHz)	ϕ_n (rad)
1	0.7692	9.035	14.92	2.4635e−6
2	0.4162	18.07	29.84	0.1600
3	0.2827	27.11	44.77	2.2149
4	0.2065	36.14	59.68	4.1903
5	0.1707	45.18	74.61	6.0510
6	0.1406	54.21	84.53	5.2671
7	0.1132	63.25	104.5	2.1070
8	0.097164	72.28	119.4	5.7511
9	0.1081	81.31	134.3	5.0005
10	0.090781	90.35	149.2	5.2319
11	0.077722	99.39	164.1	2.1679
12	0.058428	108.4	179.1	5.4738
13	0.050729	117.5	194.0	0.5649
14	0.076987	126.5	208.9	5.5812
15	0.057108	135.5	223.8	4.4043

Generally, the disturbance contains broad frequency range in front of the cone body. But most part of wave components decay gradually with down streamwise. Finally, the unstable wave only contains a special range of frequencies after a sufficient long evolution in boundary layer. In this case, a series of wave packages appear when about $s > 150$ and the total amplitude of disturbance wave grows exponentially in this range. The disturbance wave shapes have some difference for four cases of wall temperature conditions. Such evolution process agrees with traditional viewpoint of evolution of disturbance in boundary layer. Fig. 11 indicates that the amplitude of wall pressure disturbance for cold wall is not larger than that for adiabatic wall. According to Fig. 9, the starting points where the unstable waves enter into neutral curve are not same for different wall temperature conditions. This starting point for adiabatic wall is prior to that of cold wall, which leads to ahead growth of the disturbance waves. As a result, the amplitude of cold wall is smaller than that of adiabatic wall in certain streamwise range, although the growth rate is larger. For isothermal wall, the total amplitude decreases with declining wall temperature, which can be proved in Fig. 11(a)–(c). Amplitude for $T_w/T_0 = 0.5$ is the smallest, and heating surface is helpful to increasing amplitude of disturbance in boundary layer.

Fig. 12 shows the pressure disturbance along the wall surface at different intervals in streamwise. Fig. 12(a) indicates that before entering into neutral curve, the amplitudes of cold wall and adiabatic wall are almost same, (b) indicates that at the early stage after entering into the neutral curve, the amplitude of adiabatic wall exceed that of cold wall gradually, (c) indicates that after growth for a certain interval, the amplitude of adiabatic wall completely exceed the cooling wall, and (d) indicates that such situation remains to the rear of the wall surface.

Generally, cooling the surface decreases the growth of disturbance in boundary layer,while heating the surface enhances the growth of disturbance, as well as adiabatic wall case.

4.4.2. Evolution characteristic of disturbance wave

In order to study the evolution of the 15 independent disturbance waves, twelve detecting points which are used to record the time evolution of the disturbance variables on the wall surface are distributed along the streamwise. These points reflect the changing pattern of disturbance in boundary layer. Fig. 13 shows the Fourier frequency spectral analysis (FFSA) of time evolution of the pressure disturbance on these detecting points for the cold wall with $T_w/T_0 = 0.7$. In present DNS, the similar analysis has been done for the other four cases of wall temperatures. Because of similar results of FFSA (with some small difference in values), the result of $T_w/T_0 = 0.7$ is demonstrated as typical one. Fig. 13(a) shows that the low frequency waves have high amplitudes within a nose radius. This mainly because of the normal

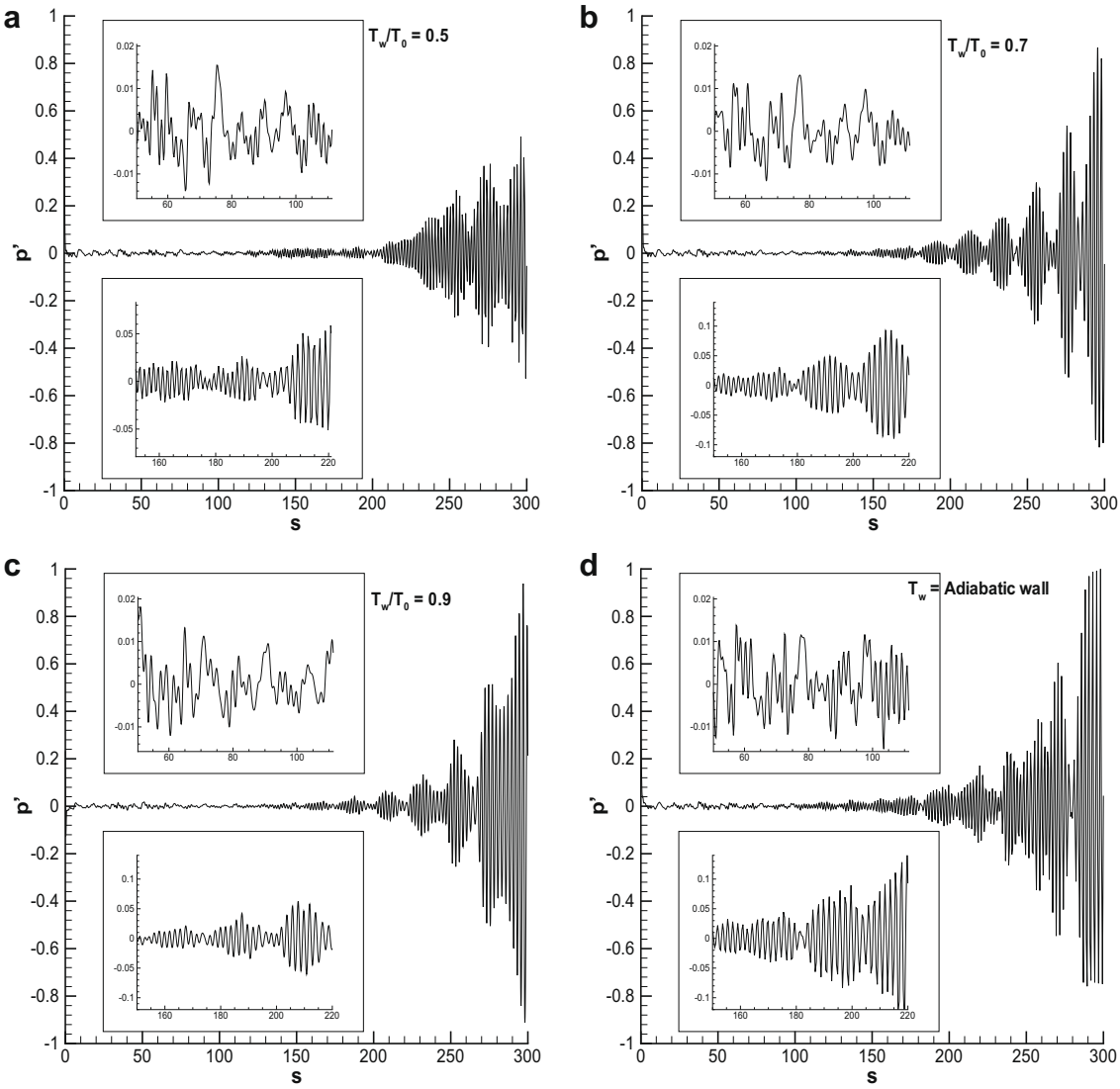

Fig. 11. Wall disturbance pressure for different wall temperature.

shock wave enlarges the forcing disturbance which have different amplitude in free-stream. Such enlargement is enhanced continuously in the shock layer where a strong oscillating wave move back and forth between normal shock and nosetip. As showed in Fig. 13(a)–(e), the FFSA amplitudes of low frequency range are larger than that of high frequency range. The low frequency components dominates disturbance development in boundary layer. Fig. 13(f)–(h) indicates that the occupancy of low frequency components and high frequency components exchange in the interval $100 \leqslant s \leqslant 137$. During this period, some disturbance wave are filtered and seldom to grow, even to decay. The FFSA amplitude of the disturbance with frequency range from about 84.53 to 134.3 kHz are almost less than 10^{-5}. When about $s > 137$, the FFSA amplitude of some high frequency components increase quickly and finally dominate the disturbance development, meanwhile the low frequency components almost are restrained to grow. Fig. 13(i)–(l) shows that the low frequency range about $f^* < 134$ kHz and the high frequency range about $f^* > 194$ kHz are very weak when about $s > 181.41$, meanwhile the moderate frequency range from about 149.1 kHz to 179.1 grows sufficiently.

In order to study the wall temperature effect on evolution of unstable mode, the similar analysis need to be done for the other four cases of wall temperature. Fig. 14 compares the FFSA amplitudes vs s for four wall temperature cases. Fig. 14(a) and (b) indicates that the amplitudes of low frequency disturbance wave at $f^* < 134.3$ kHz does not increase markedly along the streamwise. These low frequency disturbance waves belong to the first mode T–S wave which has very low growth rate. Fig. 14(c) and (d) indicates that the amplitudes increase significantly when about $s > 100$ in frequency range from about 134.3 to 179.1 kHz. These disturbance waves belong to the second unstable Mack II mode, which has larger amplitude. Fig. 14(d) and (e) indicates that the amplitudes seldom to increase along the streamwise for a high frequency range about $f^* > 180$ kHz. Some zigzag structures with very small value may caused by numerical errors. As showed in Fig. 9, these disturbance waves do not have access to the neutral curve. Based on previous analysis, the amplitude for adiabatic wall is larger than that of cold wall which can be found clearly in Fig. 14(c). Furthermore, the results of the DNS consider the whole process of disturbance development from upstream, starting from shock wave boundary, to downstream, ending at the rear of cone body, which includes the receptivity, linear growth and nonlinear growth stage. So the more accurate data reflecting the evolution of disturbance can be obtained from the DNS.

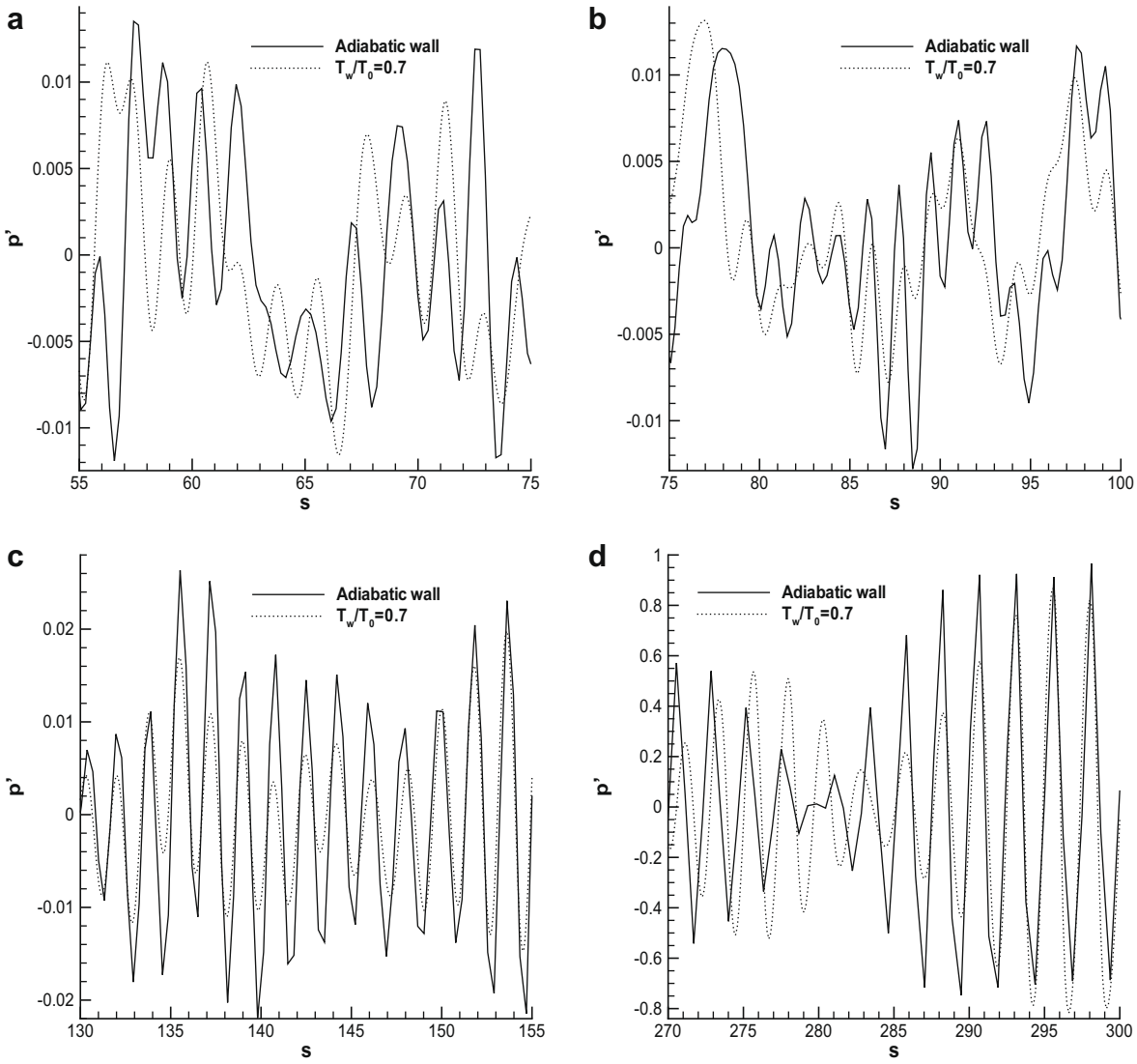

Fig. 12. Disturbance pressure for different wall temperature at different surface location for cooling and adiabatic wall.

Besides, the evolution of the disturbance along the streamwise can be divided into three intervals, S1 (about $0 < s < 11.34$), S2 (about $11.34 < s < 100$) and S3 (about $s > 100$). In the S1, the amplitudes decrease sharply from 10^{-1} order to 10^{-3}, even to 10^{-4}. In the S2, the amplitudes of disturbances are so close to each other and change slowly. Such phenomena is regarded as mode competition. Such mode competition which exist in the frequency range from about 59.68 to 179 kHz acts important roles in receptivity of hypersonic flow in a cone. The detailed analysis of such problem will be given in the subsequent paper. Kachanov [7–9], Fedorov and Khohklov [10] have proposed detail investigation in physics mechanism. In the S3, the disturbances start to grow following its own growth pattern markedly. Fig. 14(c) and (d) shows that the amplitudes of frequency range from about 134.3 to 179.1 kHz are larger than that of other's, which also are demonstrated in Fig. 13(j)–(l). Such frequency range is almost belong to the most unstable Mack II mode according to Fig. 9.

4.5. Discrepancy between results of the LST, DNS and experiment

Indeed, results of the LST indicate that cooling the surface accelerates the growth of the second unstable mode (Mack II mode) which dominates the disturbance development in boundary layer according to traditional opinion, while results of the DNS shows that the adiabatic wall enhances amplitudes of disturbances. Malik [32] has drawn the conclusion that location of the transition with adiabatic wall is dominated by the unstable first oblique T–S mode for free-stream Mach numbers up to about 7 for shape cones. For cold wall, the second unstable mode controls the growth of disturbances according to present DNS results and cooling the surface stabilizes the disturbance, which is the same as the results of the experiment [24–27,33]. So the stability mechanisms are different for cold wall and adiabatic wall, which require more investigation to clarify.

5. Conclusion

This paper proposes the effect of wall temperature on mean flow and disturbance evolution on hypersonic boundary layer over a 300 times spherical nose radius length cone with Mach number 7.99 by applying high-order shock-fitting method, and obtains some new results, as well as draws some significant conclusions.

Firstly, the number and distribution of GIPs along wall-normal are so different for cold wall and adiabatic wall (including heated wall). Especially they are significant different in favorable and adverse pressure gradient region. Those lead to different stability characteristic in boundary layer.

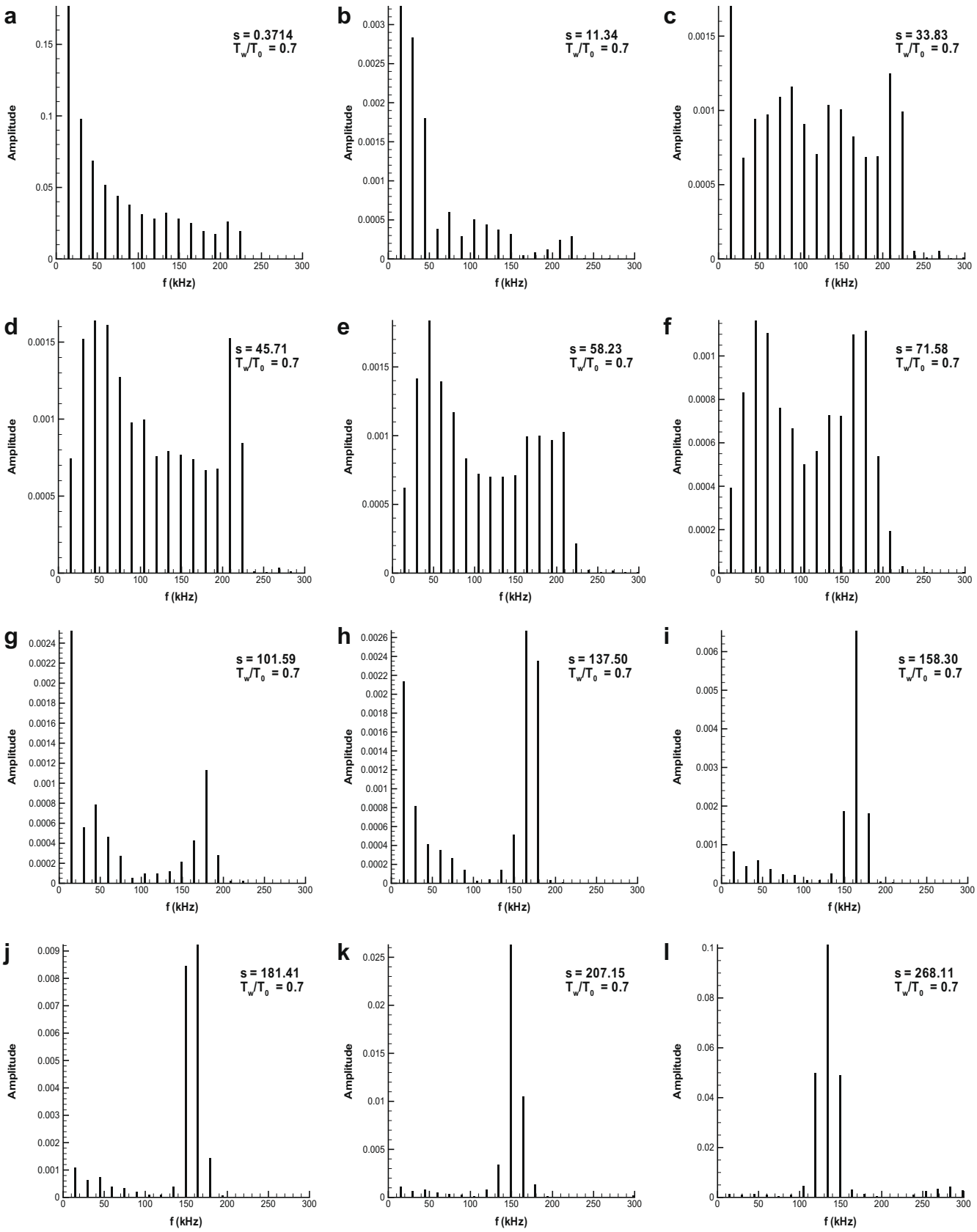

Fig. 13. Fourier frequency analysis of pressure disturbance at different surface location.

Secondly, For isothermal wall, cooling the surface accelerates the growth of Mack II, meanwhile constrains the growth of the first mode. Although cooling the surface enlarges frequency range of the disturbance to high frequency, the disturbance with very high frequency ($f^* > 179$ kHz) can not produce dominate action in boundary layer. And cooling the surface affects the distribution

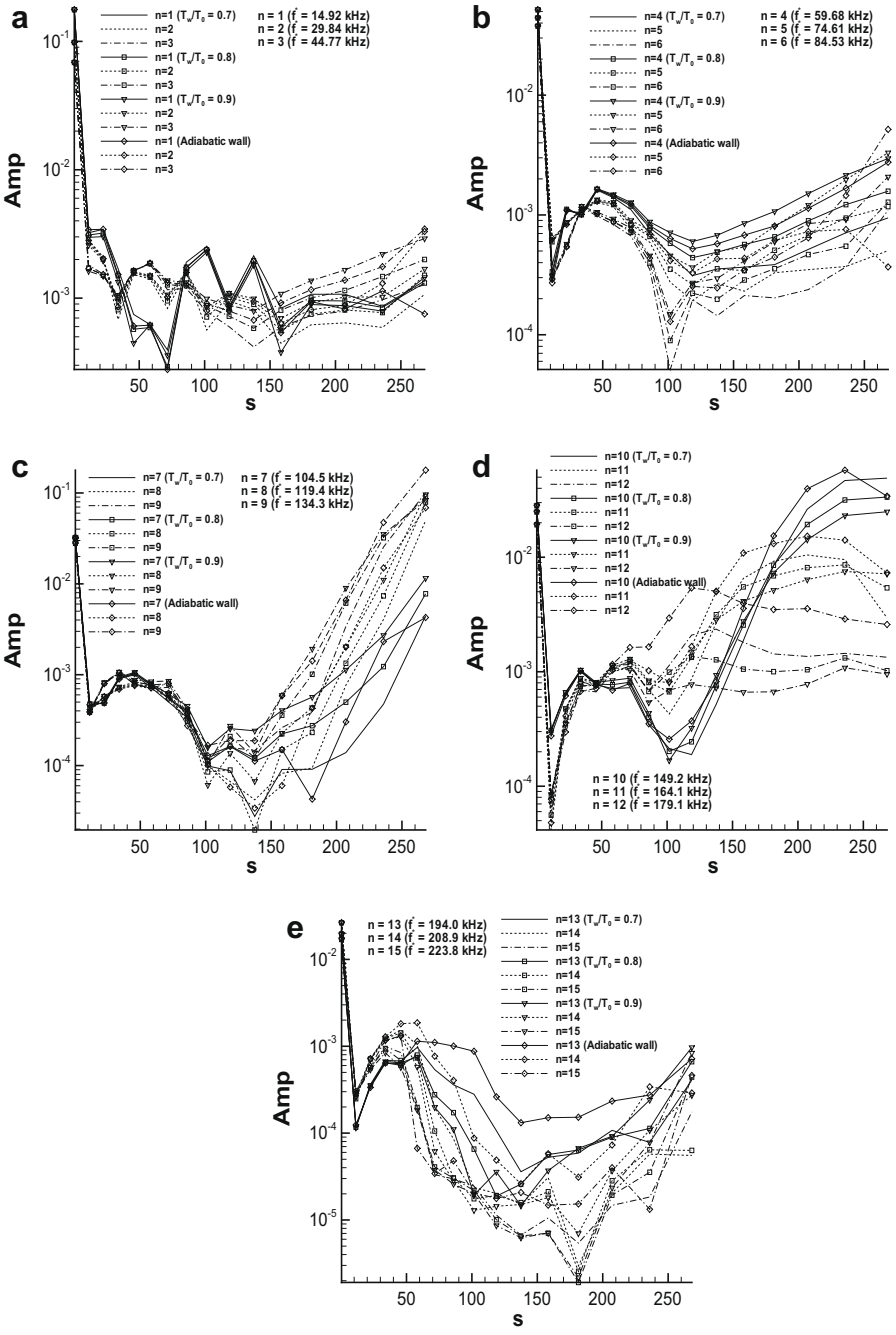

Fig. 14. Fourier frequency spectral analysis of wall surface pressure disturbance along streamwise for different temperatures.

of the disturbance wave along the normal direction. For the adiabatic wall, the growth of the disturbance does not only depend on the development of the second unstable mode.

Thirdly, the results of DNS show that mode competition exists within the disturbance with the mediate frequency range from about 59.68 to 179 kHz in the interval about $11 < s < 100$ for four wall temperature cases. Then, the disturbance with the frequency range from about 134.3 to 179.1 kHz dominate the growth of unstable wave and form the most unstable the Mack II mode.

Acknowledgements

This work was supported by National Natural Science Foundation of China (Grant Nos. 10632050, 10502052). The authors thank Shanghai Supercomputer Center (SSC) for providing computer time.

References

[1] Reed HL, Saric WS. Linear stability theory applied to boundary layers. Annu Rev Fluid Mech 1996;28:389–428.
[2] Saric WS, Reed HL, Kerschen EJ. Boundary-layer receptivity to freestream disturbances. Annu Rev Fluid Mech 2002;34:291–319.
[3] Saric WS, Reed HL, White EB. Stability and transition of three-dimensional boundary layers. Annu Rev Fluid Mech 2003;35:413–40.
[4] Saric WS. Boundary-layer stability and transition. In: Proceedings fifth international conference on numerical ship hydrodynamics; 1990. p. 23–33.
[5] Mack LM. Linear stability theory and the problem of supersonic boundary-layer transition. AIAA J 1975;13(3):278–89.
[6] Mack LM. Boundary layer linear stability theory. AGARD Rep 709; 1984, 3-1C3-81.

[7] Kachanov YS. Physical mechanisms of laminar-boundary-layer transition. Annu Rev Fluid Mech 1994;26:411–82.
[8] Borodulin VL, Gaponenko VR, Kachanov YS, et al. Late-stage transitional boundary-layer structures. Direct numerical simulation and experiment. Theor Comput Fluid Dyn 2002;15:317–37.
[9] Kachanov SK. On the resonant nature of the breakdown of a laminar boundary layer. J Fluid Mech 1987;184:43–74.
[10] Fedorov AV, Khohklov AP. Prehistory of instability in a hypersonic boundary layer. Theor Comput Fluid Dyn 2001;14:359–75.
[11] Reshotko E. Boundary layer instability, transition, and control. AIAA paper 94-0001; 1994.
[12] Morkovin MV. Transition at hypersonic speeds. NASA contractor report No. NAS1-18107; 1987. p. 5.
[13] Malik MR. Numerical methods for hypersonic boundary layer stability. J Comput Phys 1990;86:376–413.
[14] Malik MR, Spall RE, Chang CL. Effect of nose bluntness on boundary layer stability and transition. AIAA paper 90-0112; 1990.
[15] Li XL, Fu DX, Ma YW. Direct numerical simulation of boundary layer transition over a blunt cone. AIAA J 2008;46(11):2899–913.
[16] Li XL, Fu DX, Ma YW. DNS of compressible turbulent boundary layer around a sharp cone. Sci Chin G 2008;51(6):699–714.
[17] Tumin A. Three-dimensional spatial normal nodes in compressible boundary layers. J Fluid Mech 2007;586:295–322.
[18] Zhong XL. High-order finite-difference schemes for numerical simulation of hypersonic boundary-layer transition. J Comput Phys 1998;144:662–709.
[19] Zhong XL. Leading-edge receptivity to free stream disturbance waves for hypersonic flow over a parabola. J Fluid Mech 2001;441:315–67.
[20] Ma YB, Zhong XL. Receptivity of a supersonic boundary layer over a flat plate. Part 1: Wave structures and interactions. J Fluid Mech 2003;488:31–78.
[21] Ma YB, Zhong XL. Receptivity of a supersonic boundary layer over a flat plate. Part 2: Receptivity to free-stream sound. J Fluid Mech 2003;488:79–121.
[22] Ma YB, Zhong XL. Receptivity of a supersonic boundary layer over a flat plate. Part 2: Effects of different types of free-stream disturbances. J Fluid Mech 2005;532:63–109.
[23] Ma YB, Zhong XL. Boundary-layer receptivity of Mach 7.99 flow over a blunt cone to free-stream acoustic waves. J Fluid Mech 2006;556:55–103.
[24] Stetson KF, Kimmel RL. Laminar boundary layer stability experiments on a cone at Mach 8. Part 1: Blunt cone. AIAA paper 83-1761; 1983.
[25] Stetson KF, Kimmel RL. Laminar boundary layer stability experiments on a cone at Mach 8. Part 2: Blunt cone. AIAA paper 84-0006; 1984.
[26] Stetson, KF, Kimmel RL. On hypersonic boundary layer stability. AIAA paper 92-0737; 1992.
[27] Stetson KF, Kimmel RL. On the breakdown of a hypersonic laminar boundary layer. AIAA paper 93-0896; 1993.
[28] Zhang YD, Fu DX, Ma YW, Li XL. Receptivity to free-stream disturbance waves for hypersonic flow over a blunt cone. Sci China Ser G Phys Mech Astron 2008;51(11):1682–90.
[29] Su CH, Zhou H. Stability analysis and transition prediction of hypersonic boundary layer over a blunt cone with small nose bluntness at zero angle of attack. Appl Math Mech 2006;5:505–13 [in Chinese].
[30] Lees L, Lin CC. Investigation of the stability of the laminar boundary layer in compressible fluid. NACA TN 1946:1115.
[31] Herbert TH, Esfahanian V. Stability of hypersonic flow over a blunt body. AGARD CP 1993;514. 28-1C28-12.
[32] Malik MR. Prediction and control of transition in supersonic and hypersonic boundary layers. AIAA J 1998;27(11):1487–93.
[33] Potter JL. Review of the influence of cooled walls on boundary-layer transition. AIAA J 1979;18(8):1010–2.